Modelling albedo and distributed snowmelt across a low hill in Svalbard

Richard Essery[1], Eleanor Blyth[2], Richard Harding[2] and Colin Lloyd[2]

[1]Corresponding author. Institute of Geography and Earth Sciences, University of Wales, Aberystwyth SY23 3DB, UK. Tel: +44 1970 622784; Fax: +44 1970 622659; E-mail: *rie@aber.ac.uk*

[2]Centre for Ecology and Hydrology, Wallingford, OX10 8BB, UK.

Received 27 August 2004; accepted in revised form 24 January 2005

Abstract A land-surface model is used to simulate the albedo and mass of patchy snowcovers during radiation-driven melt for three years at a site in Svalbard. Performing single energy and mass balance calculations for the combined snow-covered and snow-free parts of the surface gives a faster decrease in albedo than observed because too much of the solar radiation absorbed by the composite surface is used to melt snow. Representing the snowcover separately allows the model to be calibrated to give a good match to the observed albedo for each of the years studied. A single set of model parameters cannot, however, give a good simulation for all of the years. The average snow mass and snowcover fraction measured on a grid of points can be simulated using either a distributed version of the model or a more efficient tiled version supplied with the observed relationship between snow mass and fractional coverage. Parameters obtained by optimising the snow mass simulations are more consistent from year to year than from the albedo simulations.

Keywords Snow albedo; snowcover; snowmelt; snow modelling

Nordic Hydrology **Vol 36 No 3 pp 207–218** © IWA Publishing 2005

Introduction

The presence of snow has a large effect on the energy balance of the land surface: a large fraction of the incoming solar radiation is reflected from a high albedo snow surface and the high latent heat of fusion for snow absorbs much of the available energy during melting. Through its strong influence on exchanges of energy and moisture between the surface and the atmosphere, snowcover has an important role in the global climate and has to be represented in climate models, but several studies have shown it to be a difficult quantity to model accurately and consistently (e.g. Essery *et al.* 1999b; Slater *et al.* 2001; Bowling *et al.* 2003).

Snowmelt is driven by radiation and turbulent heat transfers from the atmosphere: solar radiation is the dominant source of energy for the melting of snow persisting into the late spring or summer at high latitudes and high elevations, although turbulent fluxes are also important in mid-latitude snowmelt. Fresh snow has a high albedo, but the albedo of a snow surface decreases over time with changes in the grain structure of the snow (Wiscombe and Warren 1980) and the deposition of contaminants (Warren and Wiscombe 1980). Snow generally becomes patchy and dirty while melting, giving a surface with highly heterogeneous characteristics. Inevitably, land-surface models have to use simplified representations of snow processes and, in the case of global modelling applications, global parameters often have to be applied. Aging of snow is typically represented by making the albedo a function of the surface temperature or a function of the age and temperature history of the snow surface. Heterogeneity on scales smaller than the model resolution has to be parametrised; this is usually done through the introduction of a function relating the fraction of snowcover to the average snow depth in a gridbox. Models differ in how they perform surface flux calculations for heterogeneous snowcover: the snowcover fraction may be used

in calculating effective values for parameters such as albedo and roughness length that are then used in a single energy budget for the gridbox, as in the original version of the Met Office Surface Exchange Scheme (MOSES: Cox *et al.* 1999) for example, or separate fluxes may be calculated and then averaged using the snowcover fraction to weight the contributions from snow-covered and snow-free fractions of the gridbox, as in the Canadian Land Surface Scheme (CLASS: Verseghy 1991). This latter strategy is equivalent to the "tile model" structure adopted in MOSES 2 for heterogeneous vegetation distributions (Essery *et al.* 2003). Liston (2004) recently concluded that the use of a single energy balance for a composite surface of snow and snow-free ground leads to unrealistically rapid snowmelt.

In this paper, results from the snow model used in MOSES 2 are compared with albedo and snow depth measurements to test the ability of the model to reproduce radiation-driven snowmelt with either composite or tiled energy budgets. Snow depth measurements on a grid crossing a low hill in Svalbard and albedos measured at a point within the grid are used for these comparisons. Albedos are first simulated for three melt seasons using a composite-surface version of the snow model. Finding that this, indeed, leads to an underestimate of the period of snowcover, the simulations are then repeated using a tiled version of the model with parameters calibrated by comparison with the observations. Optimal model parameters obtained for each year are compared to see if parameters are transferable from one year to another. A distributed version of the model is used to simulate the evolving pattern of snowcover on the hill during melt for each year, and the ability of the tiled model to simulate the average snow mass and snowcover fraction on the grid is assessed. In summary, four types of simulation are performed for each year: composite and tiled albedo simulations, and distributed and tiled melt simulations.

Site description

The measurement site, described in detail by Lloyd *et al.* (2001), is on a low hill at Leirhaugen on the coastal plain 2 km west of Ny-Ålesund, Svalbard (79°56′N, 11°55′E). Clay silt with stone stripes is overlain by a thin (0.02 m) organic soil. The surface cover is a mixture of low vascular plants (*Luzula confusa*, *Saxifraga Oppositifolia*), lichens, mosses and bare soil. Measurements of albedo and snow distributions in this area have been presented previously by Bruland *et al.* (2001a, b).

The west coast of Svalbard normally receives less than 400 mm of precipitation a year, with a maximum in the autumn. Snowfall can occur at any time of the year, but a persistent snowcover is not established until September at the earliest and mid-winter melt events are common. The entire solar disc remains above the horizon at Ny-Ålesund for 129 days from 18 April to 24 August. Snowmelt typically occurs during late May and early June (Nakabayashi *et al.* 1996), although widespread snowcover can last until July (Winther *et al.* 1999) and snow patches in north-facing hollows can persist throughout the summer. The mean July temperature is 5°C, with temperatures outside the range 0–10°C being uncommon, and the majority of the energy used in snowmelt is supplied by net radiation: from eddy correlation measurements, Harding and Lloyd (1998) found that the sensible heat flux into the snow was small during melt and the latent heat flux was larger but only corresponded to a small amount of evaporation.

Downward shortwave radiation, net all-wave radiation, air temperature, humidity and wind speed were measured hourly during snowmelt in 1995, 1998 and 1999; these provide the meteorological data necessary for driving MOSES 2. Albedo was measured using upward and downward looking radiometers with cosine responses mounted on a 3 m mast; the measured albedo therefore represents some area of the surface (the base of a 45° cone of height 3 m has an area of 28.3 m^2).

Snow depths were measured on a grid of 66 (11 × 6) snow stakes with 10 m spacing in 1995 and 52 (13 × 4) stakes with 20 m spacing in 1998 and 1999. The long axes of the grids ran north to south over the hill. Measurements were made daily or every other day from 30 May 1995, 9 June 1998 and 19 May 1999. Figure 1 shows the latter locations of the snow stakes on a contour map of the topography, with shading showing the measured snow depth on 9 June 1998. Although the slopes are very gentle, there is a strong spatial variation in snow accumulation because of microtopography: the summit of the hill was free of snow, while the deepest snow lay in drifts exceeding 80 cm in depth near the summit and at the base of the hill to the north. Depths were converted to snow water equivalent (SWE, in $\mathrm{kg\,m^{-2}}$ or mm) using the average measured density of $420\,\mathrm{kg\,m^{-3}}$. Daily measurements in snow pits near the grid showed a gradual increase in density from $370\,\mathrm{kg\,m^{-3}}$ on 4 June 1998 to $500\,\mathrm{kg\,m^{-3}}$ by the end of the month (O. Bruland, personal communication).

Model description

MOSES 2 calculates snow albedo either as a function of temperature (Cox *et al.* 1999) or using a simplification of the Marshall (1989) parametrisation of the Wiscombe and Warren (1980) spectral snow albedo model. For the latter option, aging of snow is characterised by a prognostic grain size, r, set to $r_0 = 50\,\mu\mathrm{m}$ for fresh snow and limited to a maximum value of $2000\,\mu\mathrm{m}$. The change in r over a timestep from time t to $t + \Delta t$ is given by

$$r(t+\Delta t) = \left[r(t)^2 + \frac{G_r}{\pi}\Delta t\right]^{1/2} - [r(t) - r_0]\frac{S_f \Delta t}{d_0} \tag{1}$$

where S_f is the snowfall rate and d_0, the mass of fresh snow required to refresh the albedo, is set to $2.5\,\mathrm{kg\,m^{-2}}$. The empirical grain *area* growth rate is

$$G_r = \begin{cases} 0.6 & T_* = T_m \ \text{(melting snow)} \\ 0.06 & T_* < T_m, r < 150\,\mu\mathrm{m} \ \text{(cold fresh snow)} \\ 0.01 & T_* < T_m, r > 150\,\mu\mathrm{m} \ \text{(cold aged snow)} \end{cases} \tag{2}$$

for surface temperature T_* and melting point T_m. Snow albedos are calculated as

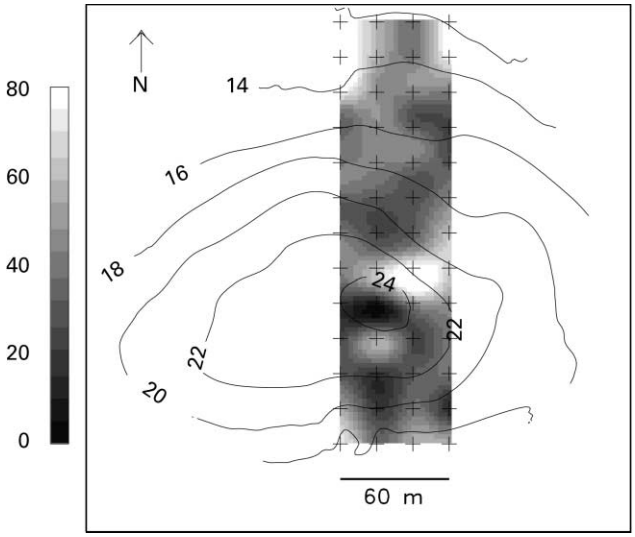

Figure 1 Topographic map of the study site with a 2 m contour interval, showing the location of snow stakes (crosses) and snow depths in cm on 9 June 1998 (shading)

$$\alpha_s = \alpha_{fs} - 0.001\left(r^{1/2} - r_0^{1/2}\right) - 0.045\ \ln\left(\frac{r}{r_0}\right) \tag{3}$$

where α_{fs} is the albedo of fresh snow. The two terms involving r on the right of Eq. (3) represent separate visible and near-infrared albedos that are simply averaged here. The full parametrisation includes the influences of soot in the snow and zenith angle, but these refinements are not used here. With α_{fs} set to 0.84 by default, α_s approaches minima of 0.79 for cold snow and 0.64 for melting snow.

The average albedo of a partially snow-covered surface with snow albedo α_s and snow-free albedo α_0 is given by

$$\alpha = f\alpha_s + (1 - f)\alpha_0 \tag{4}$$

where the fraction of snowcover is parametrised as

$$f = \frac{S}{S + A} \tag{5}$$

for SWE S. A is an adjustable parameter; in MOSES 2, this is taken to be a function of surface roughness on the assumption that a greater depth of snow is required to mask the albedo of a rougher surface (Essery *et al.* 2003). Although the parameters A, α_{fs}, α_0 and roughness length z_0 are normally specified in MOSES 2, α_0 is determined here from observations after snowmelt and the other parameters are taken as independent and adjustable.

For given downward shortwave and longwave radiative fluxes $SW_\downarrow$ and $LW_\downarrow$, the energy balance of the snow surface is

$$(1 - \alpha)SW_\downarrow + LW_\downarrow - \sigma T_*^4 = H + LE + G + M \tag{6}$$

where σ is the Stefan–Boltzmann constant, H and LE are sensible and latent heat fluxes to the atmosphere, G is the heat flux into the snow and M is the heat flux used in melting snow. Equation (6) is used along with flux parametrisations to calculate the snow surface temperature and melt rate (Essery *et al.* 2003).

MOSES 2 represents partial snowcover as a composite surface of snow and snow-free ground with the albedo in Eq. (6) given by Eq. (4). The SWE is updated each timestep by applying an increment

$$\Delta S = (S_f - LE/L_s - M/L_f)\Delta t \tag{7}$$

where L_s is the latent heat of sublimation and L_f is the latent heat of fusion. An alternative model structure is also implemented here with separate energy balances for snow and snow-free ground. For the snow tile, Eq. (7) is replaced by

$$\Delta S = (S_f - fLE/L_s - fM/L_f)\Delta t \tag{8}$$

for the increment in area-average SWE and α in Eq. (6) is given by

$$\alpha = \alpha_s + (\alpha_0 - \alpha_s)e^{-0.2S}. \tag{9}$$

This weighted albedo approaches α_s for deep snow but allows for the absorption of solar radiation by the ground underlying shallow snow and reduces the documented tendency of tiled snow models to retain very small snow fractions (Slater *et al.* 2001).

Albedo simulations

Hourly albedo measurements often show significant diurnal variations because of factors such as the zenith angle dependence of snow albedos, the influences of cloud cover and

shadows, and any slight errors in the levelling of radiometers. To focus on the decay of albedo during melt, Figure 2 shows effective daily albedos (diamonds) calculated by dividing the total reflected solar radiation each day by the incoming total. For each year, the albedo could be well approximated by a slow linear premelt decrease in albedo, a fast linear decrease as the fraction of snowcover decreases during active melt and a constant snow-free albedo after melt, as suggested by Gray and Landine (1987).

The measured initial SWE near the radiometers was 73 mm on 30 May 1995, 169 mm on 14 June 1998 and 165 mm on 19 May 1999. MOSES 2 simulations using a single energy balance, with α_s matched to initial measurements of the albedo, give reasonable matches to the observed albedo during the early stages of melt, as shown by the dashed lines in Figure 2. Once an appreciable fraction of snow-free ground has appeared, however, the reduced albedo and increased absorption of solar radiation lead to accelerating melt: the snow disappears and the simulated albedo drops to the albedo of the snow-free ground much sooner than observed. Too much of the net radiation absorbed by the combined snow and snow-free fractions of the surface is used to melt snow. Although heat from the snow-free ground may be advected to the snow through the atmosphere (Liston 1995; Essery 1997), this is implicitly included in the observed air temperature and is unlikely to be significant in situations where the surface energy budget is dominated by radiative rather than turbulent fluxes.

Simulations using separate surface energy balance calculations for snow and snow-free ground with appropriate parameter values give better results, as shown by the solid lines in Figure 2. Because the net radiation is much greater than the sensible and latent heat fluxes, the results are rather insensitive to the choice of z_0. Changes in area-average albedo are

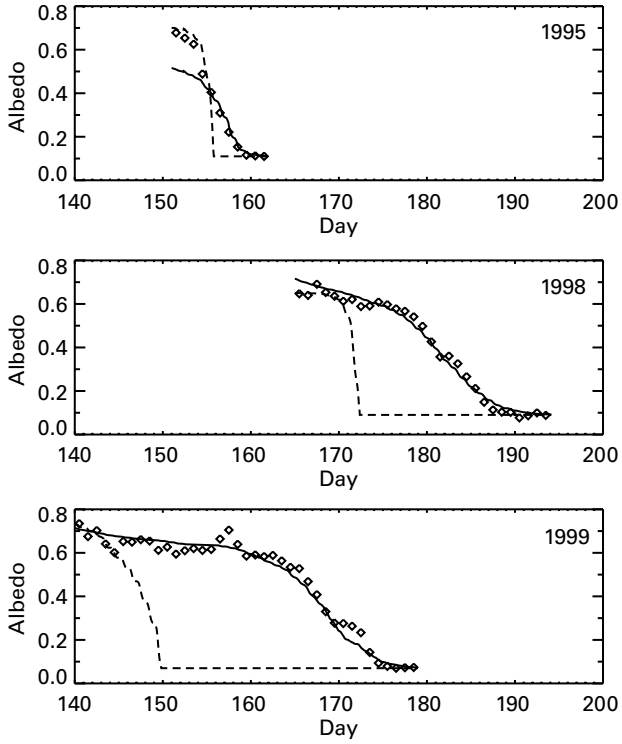

Figure 2 Albedo from observations (◇), simulations with a single surface energy balance (dashed lines) and simulations using optimised parameters in a tile model with separate energy balances for snow and snow-free ground (solid lines)

dominated by changes in the fraction of snowcover, rather than changes in snow albedo, so the results are also insensitive to the rate of snow aging. The onset of rapid snowcover depletion is determined by α_{fs} and the width of the albedo decay curve is determined by A, largely independent of each other; there is therefore a unique choice of these two parameters giving the lowest root mean square error in the simulated albedo without the "equifinality" found in more sophisticated models (Beven and Franks 1999) or even in simple model simulations of SWE (Essery and Etchevers 2004). Tuning the parameters to minimise the albedo error, the best results for 1998 and 1999 are obtained using very similar values of A and α_{fs}: 37 mm and 0.9 for 1998; 36 mm and 0.9 for 1999. These values of A correspond to a roughness length of around 15 mm in the MOSES 2 parametrisation: in comparison, measurements for short tundra vegetation in Svalbard have given roughness lengths of 3 mm for a flat moss and lichen site (Lloyd *et al.* 2001) and 21 mm for tussocks (Harper and Wiseman 1977). The fresh snow albedos are a little higher than the default value used in the global implementation of MOSES 2, as might be expected for clean Arctic snow, but optimised albedo values also depend on model structure (Essery and Etchevers 2004).

For 1995, the albedo measurements suggest that there was an early and rapid melt. The minimum error in the albedo simulation is given by $A = 18$ mm and $\alpha_{fs} = 0.67$, rather different from the values obtained for 1998 and 1999. Measurements of snow contamination are not available to test the possibility that the shallower snowcover in 1995 was dirtier than in the other years. Warm periods and rain during May 1995, preceding the start of the simulation period, will also have influenced the snow structure. Even after optimisation, the parameters required to match the rapid melt in 1995 give an underestimate of the initial albedo. It may be that the composite energy balance is a more appropriate representation for the initial melt stages of a shallow snowcover with small patches of exposed ground.

Snowcover simulations

Averages, standard deviations and coefficients of variation (standard deviation divided by the average) of gridded SWE measurements for the initial measurement dates in 1995, 1998 and 1999 are given in Table 1. Several studies (e.g. Donald *et al.* 1995; Shook 1995; Essery *et al.* 1999a) have found that distributions of SWE over reasonably homogeneous surfaces can be approximated by a lognormal distribution, so the logarithm of SWE can be approximated by a normal distribution. In Figure 3, the cumulative distribution $F(S)$ of initial SWE for each year is plotted against the scaled logarithm $(\ln\ s - \bar{y})/\sigma_y$, where $\bar{y}$ is the average of $y\ =\ \ln S$ and σ_y is its standard deviation. The line in Figure 3 is a cumulative normal distribution with zero mean and unit standard deviation for comparison; the measured distributions all lie close to this theoretical distribution.

From gridded SWE measurements, the fraction of snowcover on each measurement date can be estimated by counting the number of points at which snow remains and dividing by the total number of grid points. Observed snowcover fractions and average SWE are plotted against each other for each year in Figure 4. The resulting snowcover depletion curves are fairly consistent from year to year, in agreement with the results of Luce and Tarboton (2004), but they do not fit the curves used in the albedo simulations (dashed line), which give

Table 1 Averages, standard deviations and coefficients of variation of SWE measured on grids

Date	Average SWE (mm)	SWE standard deviation (mm)	Coefficient of variation
30 May 1995	107	67	0.63
9 June 1998	180	83	0.46
19 May 1999	173	70	0.40

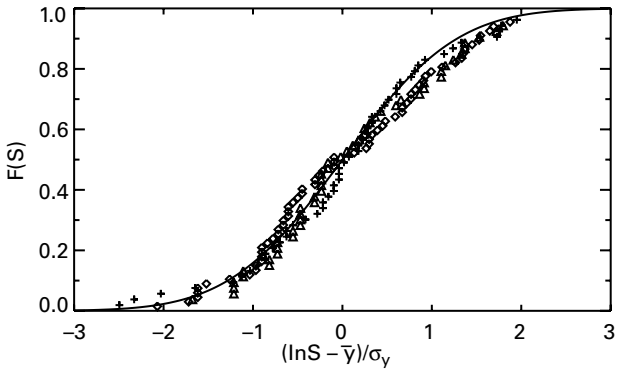

Figure 3 Scaled distributions of the logarithm of initial SWE from grid measurements in 1995 (◇), 1998 (+) and 1999 (△), compared with a normal distribution (line)

an underestimate of the coverage for deep snow. A better fit is given by the alternative function

$$f = \tanh\left(\frac{S}{B}\right) \tag{10}$$

where B is an adjustable parameter determining the width of the snowcover depletion curve. This functional form was found to give a good approximation to observed snowcover fractions in previous studies (Baker *et al.* 1991; Yang *et al.* 1997) and was shown to be consistent with the lognormal SWE distribution by Essery and Pomeroy (2004). A reasonable match is obtained for all years using $B = 50$ mm, as shown by the solid line in Figure 4, although better results can be obtained by using different values of B for each year. Without further information on the distribution of snow within the downward-looking radiometer's field of view, it is not clear why a single function cannot be used to match observations of both the average albedo and the snowcover fraction (photographs from a downward-looking camera with a hemispheric lens mounted alongside a radiometer would provide useful information). It should be remembered, however, that the "extent" and "support" (Western and Blöschl 1999) of these measurements are different and depletion curves derived from them need not be the same: the albedo measurements are effective values averaged over some area, whereas the snowcover fraction is derived from point measurements over a larger area. A formulation such as Eq. (5) which gives incomplete snowcover even for deep snow may be more appropriate for large-scale models, the gridboxes of which will enclose more variability; Roesch *et al.* (2001) used Eq. (10) for

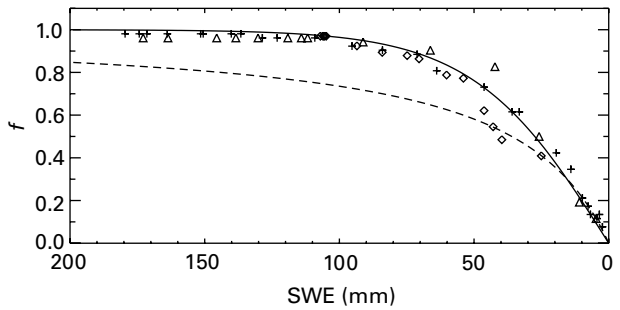

Figure 4 Observed snowcover depletion curves for 1995 (◇), 1998 (+) and 1999 (△), compared with fitted curves from Eq. (5) with $A = 36$ mm (dashed line) and Eq. (10) with $B = 50$ mm (solid line)

fractional snowcover on flat surfaces, multiplied by the square root of Eq. (5) for gridboxes with significant subgrid orography in a climate model.

Observations of average SWE and snowcover fraction on the grids are plotted against date and against each other in Figures 5, 6 and 7 for 1995, 1998 and 1999, respectively. Comparing Figures 2 and 5 shows that the snow had disappeared under the radiometers by day 160 in 1995, but 77% (51 out of 66) of the grid points still had snow on that date. Discrepancies in the timing of snow disappearance inferred from albedo and grid measurements are not so large for 1998 and 1999.

The pattern of snowcover can be simulated using a distributed version of MOSES 2 with separate calculations of SWE for each point on the measurement grid. For point simulations, the distributed model has a single adjustable parameter: the fresh snow albedo. Optimising simulations of the average SWE against observations, the best results are obtained with the values of α_{fs} given in the first column of Table 2. The dashed lines in Figures 5, 6 and 7 show results from these simulations. The simulated values of SWE lie very close to the observations, but simulated snowcover fractions initially decrease too rapidly in 1998 and 1999, and the simulated snowcover depletion curves lie below the observed curves. The distributed model gives nearly homogeneous melt rates across the grid, but an actual depletion curve lying above the theoretical curve for homogeneous melt is a signature of deeper snow melting faster than shallow snow (Essery and Pomeroy 2004). The 5° slopes are too gentle to cause much variation in solar radiation at the surface and the deepest snow lies in a drift on a northeast-facing slope anyway. As the drift is downwind of a scoured region, the increased melt could be because of advection of heat from bare ground or, more likely, in

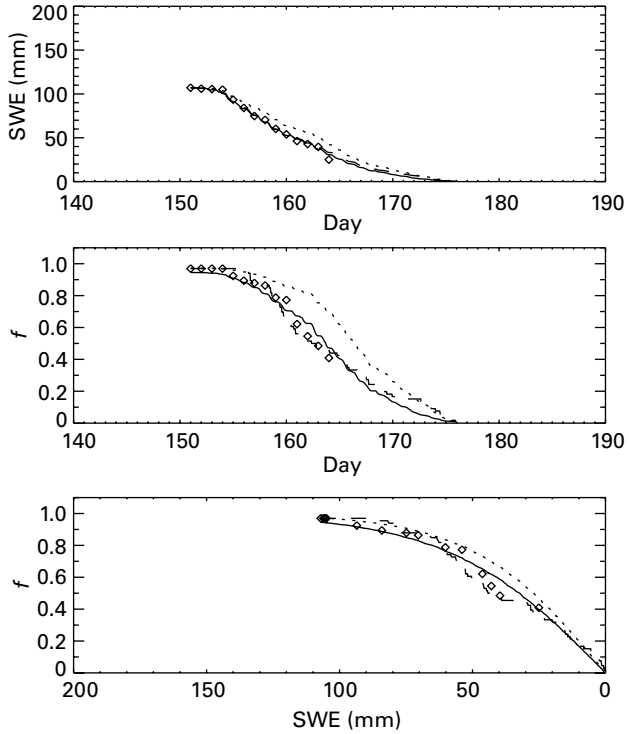

Figure 5 Average SWE and snowcover fraction plotted against date and against each other for 1995. Diamonds are from gridded observations, dashed lines are from the distributed version of MOSES 2, solid lines are from the tiled version with parameters optimised for each year and dotted lines are from the tiled version with average parameters

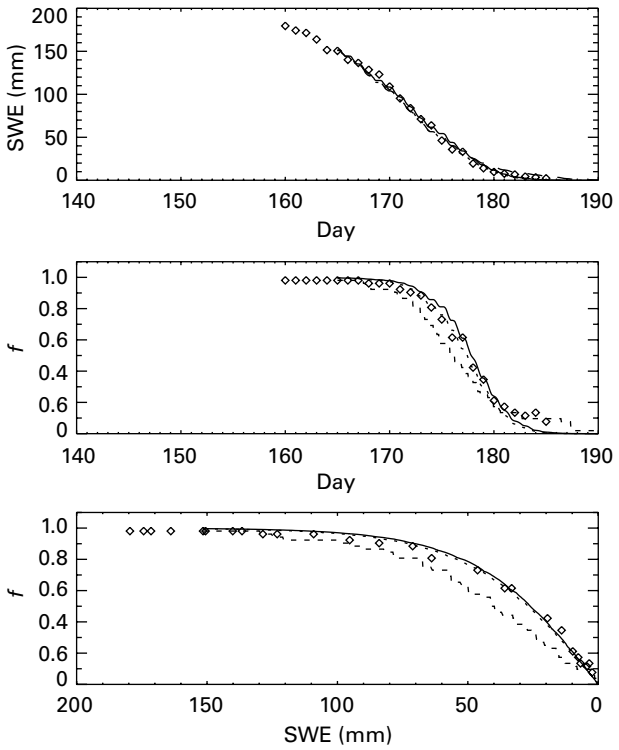

Figure 6 Average SWE and snowcover fraction plotted against date and against each other for 1998. Diamonds are from gridded observations, dashed lines are from the distributed version of MOSES 2, solid lines are from the tiled version with parameters optimised for each year and dotted lines are from the tiled version with average parameters

radiation-driven melt because of dust blown onto the snow surface reducing the albedo. Better simulations of the snowcover depletion curve can be obtained by specifying a spatial variation in albedo across the grid, but without independent information on variations in the surface energy balance this is a rather contrived procedure.

With measurements of both f and S available, the parameter B in Eq. (10) can be optimised for use in the tiled version of MOSES 2: Table 2 gives values for each year, which turn out to be nearly proportional to the coefficients of variation listed in Table 1. Subsequently optimising the fresh snow albedo, good simulations can be obtained for both average SWE and snowcover fraction for all years, as shown by the solid lines in Figures 5, 6 and 7. The tiled version of the model is much more computationally efficient than the distributed version, but information on the snowcover depletion curve has to be supplied. The optimised parameters given in Table 2 are more consistent from year to year than they were for the albedo simulations discussed above. Dotted lines in Figures 5, 6 and 7 show that fairly good simulations can be obtained using the average values from Table 2 as a single parameter set for all years, although the snow then melts a little too slowly in 1995 and too quickly in 1998.

Conclusions

Because the energy budget of a surface depends strongly on albedo and the albedo of a partially snow-covered surface depends strongly on the fraction of snowcover, comparisons with albedos measured over an area during radiation-driven melt provide a much sterner test of a snow model than the common procedure of comparing simulated SWE with

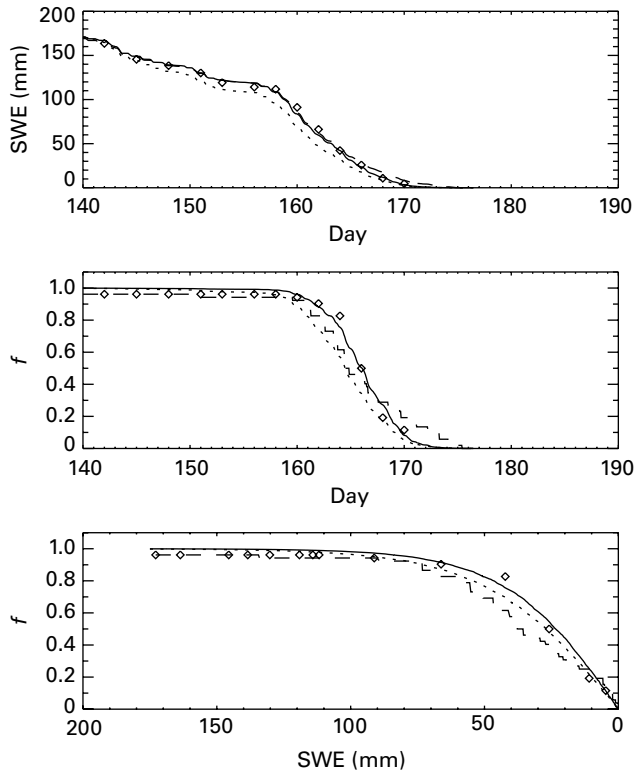

Figure 7 Average SWE and snowcover fraction plotted against date and against each other for 1999. Diamonds are from gridded observations, dashed lines are from the distributed version of MOSES 2, solid lines are from the tiled version with parameters optimised for each year and dotted lines are from the tiled version with average parameters

measurements at a point (Essery *et al.* 1999b; Slater *et al.* 2001; Essery and Etchevers 2004). The snow model of the MOSES 2 land-surface scheme was used here in several configurations to simulate albedo and snowcover during melt on a low hill in the Arctic. Performing a single surface energy budget for both snow-covered and snow-free ground removed the snow too early. For simulations with a separate budget for snow, the model parameters could be calibrated to give good simulations of the observed albedo. The optimised parameters were very similar for two years (1998 and 1999) with similar initial snowdepths and similar to the default parameters used in MOSES 2 without calibration, but rather different parameters had to be used for another year (1995) with a shallower snowpack and earlier melt. It is unlikely that *any* model could estimate parameters *a priori* for all three

Table 2 Optimised parameters for simulations of average SWE with the distributed and tiled versions of MOSES 2

Year	Distributed	Tiled	
	α_{fs}	α_{fs}	B
1995	0.85	0.84	60
1998	0.87	0.89	48
1999	0.90	0.90	43
Mean	0.88	0.88	50

years without additional information on the initial distribution and contamination of the snow that was not available in this study.

Area-average albedos are dominated by the emergence of snow-free ground and the measurements used here do not contain sufficient information for the calibration of model parameters determining the rates of decrease in spectral snow albedos with age. The influence of aging on albedo is, however, important for the energy balance of snow. Information on snow aging can be obtained using narrow-beam and spectral radiometers viewing continuous snow patches (Winther *et al.* 1999).

A distributed snowmelt simulation with homogeneous snow albedos matched the average SWE measured on a grid reasonably well but did not simulate the observed relationship between SWE and the fraction of snowcover well because the observed melt rate was not homogeneous: deeper snow melted faster, possibly as a result of contamination by dust blown off scoured areas. Optimising the model's snow albedo at each point could give an improved simulation, but at the expense of introducing extra parameters. Trampling of the snow while making the depth measurements will, itself, have influenced the albedo and melt rate of the snow to some extent.

If simulations of average SWE and fractional cover only are required, rather than detailed distributions, a tiled model can give a reasonable match to the observations without the expense of using a distributed model. Optimised model parameters were more consistent from year to year for snowcover simulations than for albedo simulations at the site studied here. Representing average SWE and fractional cover is a greater problem for areas with significant relief. Several models have used a partially distributed approach, dividing mountainous regions into elevation bands (Arola and Lettenmaier 1996; Liston *et al.* 1999; Essery 2003).

Acknowledgements

RE is supported by NERC Advanced Research Fellowship NER/J/S/2001/00812. The MOSES 2 code was provided by the Met Office. Snow pit data were supplied by Oddbjørn Bruland. Tim Kyte and Nick Cox assisted with the measurement of snow depths.

References

Arola, A. and Lettenmaier, D.P. (1996). Effects of subgrid spatial heterogeneity on GCM-scale land surface energy and moisture fluxes. *J. Clim.*, **9**, 1339–1348.

Baker, D.G., Skaggs, R.H. and Ruschy, D.L. (1991). Snow depth required to mask the underlying surface. *J. Appl. Meteorol.*, **30**, 387–392.

Beven, K.J. and Franks, S.W. (1999). Functional similarity in landscape scale SVAT modelling. *Hydrol. Earth Syst. Sci.*, **3**, 85–93.

Bowling, L.C., *et al.* (2003). Simulation of high latitude hydrological processes in the Torne-Kalix basin: PILPS Phase 2e. 1: Experiment design and summary intercomparisons. *Global Planet. Change*, **38**, 1–30.

Bruland, O., Marechal, D., Sand, K. and Killingtveit, A. (2001a). Energy and water balance studies of a snow cover during snowmelt period at a high arctic site. *Theor. Appl. Climatol.*, **70**, 53–63.

Bruland, O., Sand, K. and Killingtveit, A. (2001). Snow distribution at a high Arctic site at Svalbard. *Nord. Hydrol.*, **32**, 1–12.

Cox, P.M., Betts, R.A., Bunton, C.B., Essery, R.L.H., Rowntree, P.R. and Smith, J. (1999). The impact of new land surface physics on the GCM simulation of climate and climate sensitivity. *Clim. Dyn.*, **15**, 183–203.

Donald, J.R., Soulis, E.D., Kouwen, N. and Pietroniro, A. (1995). A land cover-based snow cover representation for distributed hydrologic models. *Wat. Res. Res.*, **31**, 995–1009.

Essery, R.L.H. (1997). Modelling fluxes of momentum, sensible heat and latent heat over heterogeneous snowcover. *Q. J. R. Meteor. Soc.*, **123**, 1867–1883.

Essery, R.L.H. (2003). Aggregated and distributed modelling of snowcover for a high-latitude basin. *Global Planet. Change*, **38**, 161–164.

Essery, R.L.H. and Etchevers, P. (2004). Parameter sensitivity in simulations of snowmelt. *J. Geophys. Res.*, **109,** doi:10.1029/2004JD005036.

Essery, R.L.H. and Pomeroy, J.W. (2004). Implications of spatial distributions of snow mass and melt rate on snowcover depletion: theoretical considerations. *Ann. Glaciol.*, **38**, 261–265.

Essery, R.L.H., Best, M.J., Betts, R.A., Cox, P.M. and Taylor, C.M. (2003). Explicit representation of subgrid heterogeneity in a GCM land-surface scheme. *J. Hydrometeor.*, **4**, 530–543.

Essery, R.L.H., Li, L. and Pomeroy, J.W. (1999a). A distributed model of blowing snow over complex terrain. *Hydrol. Processes*, **13**, 2423–2438.

Essery, R.L.H., Martin, E., Douville, H., Fernández, A. and Brun, E. (1999). A comparison of four snow models using observations from an alpine site. *Clim. Dyn.*, **15**, 583–593.

Gray, D.M. and Landine, P.G. (1987). Albedo model for shallow prairie snow covers. *Can. J. Earth Sci.*, **24**, 1760–1768.

Harding, R.J. and Lloyd, C.R. (1998). Fluxes of water and energy from three high latitude tundra sites in Svalbard. *Nord. Hydrol.*, **29**, 267–284.

Harper, J.R. and Wiseman, W.J. (1977). Temporal variation of surface roughness over a tundra surface. *J. Geophys. Res.*, **82**, 3495–3497.

Liston, G.E. (1995). Local advection of momentum, heat and moisture during the melt of patchy snow covers. *J. Appl. Meteor.*, **34**, 1705–1715.

Liston, G.E. (2004). Modelling regional and global scale subgrid heterogeneous snow cover. *J. Clim.*, **17**, 1381–1397.

Liston, G.E., Pielke, R.A. and Greene, E.M. (1999). Improving first-order snow-related deficiencies in a regional climate model. *J. Geophys. Res.*, **104**, 19559–19567.

Lloyd, C.R., Harding, R.J., Friborg, T. and Aurela, M. (2001). Surface fluxes of heat and water vapour from sites in the European arctic. *Theor. Appl. Climatol.*, **70**, 19–33.

Luce, C.H. and Tarboton, D.G. (2004). The application of depletion curves for parametrization of subgrid variability of snow. *Hydrol. Processes*, **18**, 1409–1422.

Marshall, S.E. (1989). A physical parametrization of snow albedo for use in climate models. *NCAR Cooperative Thesis* 123, National Center for Atmospheric Research, Boulder, CO.

Nakabayashi, H., Kodama, Y., Takeuchi, Y., Ozeki, T. and Ishikawa, N. (1996). Characteristics of heat balance during snowmelt season in Ny-Ålesund, Spitsbergen island. *Mem. National Institute of Polar Research, Special Issue*, **51**, 255–266.

Roesch, A.H., Gilgen, M., Wild, M. and Ohmura, A. (2001). A new snow cover fraction parametrization for the ECHAM4 GCM. *Clim. Dyn.*, **17**, 933–945.

Shook, K. (1995). Simulation of the ablation of prairie snowcovers. *PhD Thesis*, University of Saskatchewan.

Slater, A.G. *et al.* (2001). The representation of snow in land surface schemes: results from PILPS 2(d). *J. Hydrometeor.*, **2**, 7–25.

Verseghy, D.L. (1991). CLASS – a Canadian land surface scheme for GCMs. *Int. J. Climatol.*, **11**, 111–133.

Warren, S.G. and Wiscombe, W.J. (1980). A model for the spectral albedo of snow. II. Snow containing atmospheric aerosols. *J. Atmos. Sci.*, **37**, 2734–2745.

Western, A.W. and Blöschl, G. (1999). On the spatial scaling of soil moisture. *J. Hydrol.*, **217**, 203–224.

Winther, J.-G., Gerland, S., Orbaek, J.B., Ivanov, B., Blanco, A. and Boike, J. (1999). Spectral reflectance of melting snow in a high Arctic watershed on Svalbard: some implications for optical satellite remote sensing studies. *Hydrol. Processes*, **13**, 2033–2049.

Wiscombe, W.J. and Warren, S.G. (1980). A model for the spectral albedo of snow. I. Pure snow. *J. Atmos. Sci.*, **37**, 2712–2733.

Yang, Z.-L., Dickinson, R.E., Robock, A. and Vinnikov, K.Y. (1997). On validation of the snow sub-model of the Biosphere-Atmosphere Transfer Scheme with Russian snow cover and meteorological observational data. *J. Clim.*, **10**, 353–373.